

## AN EMPIRICAL METHOD FOR IMPROVING THE QUALITY OF *RXTE* HEXTE SPECTRA

JAVIER A. GARCÍA<sup>1</sup>, VICTORIA GRINBERG<sup>2</sup>, JAMES F. STEINER<sup>1,2</sup>, JEFFREY E. MCCLINTOCK<sup>1</sup>, KATJA POTTSCHMIDT<sup>3,4</sup>,  
RICHARD E. ROTHSCCHILD<sup>5</sup>  
*Draft version March 10, 2021*

### ABSTRACT

We have developed a correction tool to improve the quality of *RXTE* HEXTE spectra by employing the same method we used earlier to improve the quality of *RXTE* PCA spectra. We fit all of the hundreds of HEXTE spectra of the Crab individually to a simple power-law model, some 37 million counts in total for Cluster A and 39 million counts for Cluster B, and we create for each cluster a combined spectrum of residuals. We find that the residual spectrum of Cluster A is free of instrumental artifacts while that of Cluster B contains significant features with amplitudes  $\sim 1\%$ ; the most prominent is in the energy range 30–50 keV, which coincides with the iodine K edge. Starting with the residual spectrum for Cluster B, via an iterative procedure we created the calibration tool HEXBCORR for correcting any Cluster B spectrum of interest. We demonstrate the efficacy of the tool by applying it to Cluster B spectra of two bright black holes, which contain several million counts apiece. For these spectra, application of the tool significantly improves the goodness of fit, while affecting only slightly the broadband fit parameters. The tool may be important for the study of spectral features, such as cyclotron lines, a topic that is beyond the scope of this paper.

*Subject headings:* instrumentation: detectors – space vehicles: instruments – X-ray: individual (Crab, XTE J1752–223, GX 339–4)

### 1. INTRODUCTION

The *Rossi X-ray Timing Explorer (RXTE)* was launched into a low earth orbit on 30 December 1995 and operated continuously until the mission was terminated on 4 January 2012. The three instruments aboard *RXTE* were (i) the All Sky Monitor (ASM; Levine et al. 1996), which consisted of three coded aperture cameras that scanned about  $\sim 80\%$  of the sky every orbit; (ii) the Proportional Counter Array (PCA; Jahoda et al. 2006), a set of five proportional counter detectors sensitive over the energy range 2–60 keV; and (iii) the High Energy X-ray Timing Experiment (HEXTE; Rothschild et al. 1998), which consisted of two independent clusters (A and B), each with four NaI(Tl)/CsI(Na) phoswich scintillation detectors sensitive over the energy range 15–250 keV. It is the calibration of the latter instrument that is the focus of this paper. A detailed discussion of the HEXTE detectors can be found in Rothschild et al. (1998) and references therein; here, we provide a brief overview.

Each of the eight HEXTE detectors was fitted with a lead honeycomb collimator giving a  $1^\circ$  FWHM field of view. All eight collimators were co-aligned on source. The net open area of the eight detectors was  $\sim 1600$  cm<sup>2</sup> with an average energy resolution of 15.4% FWHM at

60 keV. Both clusters A and B achieved a near-real-time estimate of the background by being rocked between the source and a background field through an angle of  $1:5$ ; the rocking axes of the clusters were orthogonal. The exposure time on source was 32 s, except early in the mission when it was 16 s. The corresponding observation times on the background were 28 s and 12 s, respectively.

We improve the calibration of the HEXTE using precisely the same approach we used previously for the PCA (García et al. 2014). Namely, for each cluster separately we fit individually all of the HEXTE spectra of the Crab, which we assume to be featureless, to a simple power-law model. We then combine the residual spectra to create two master spectra that have extreme statistical precision. We find that the spectrum of Cluster B contains prominent instrumental artifacts, while the spectrum of Cluster A is essentially free of such artifacts. Via an iterative process, we create the calibration tool HEXBCORR, and we demonstrate the effectiveness of the tool in correcting the spectra of two bright black holes. It is especially important to perform this correction in studying spectra with high signal-to-noise, e.g., spectra of bright sources and/or spectra created by combining several data sets. We suggest that it may also be important for the study of spectral features, such as cyclotron lines.

### 2. FITS TO CRAB SPECTRA AND THE CREATION OF A RATIO SPECTRUM FOR CLUSTER B

The performance of the HEXTE was affected by three major events during the 16-year mission<sup>6</sup>. (1) On 1996 March 6, the pulse height analyzer in one of the detectors of Cluster B failed so that after that date only three of the four detectors were serviceable. (2) In October

<sup>1</sup> Harvard-Smithsonian Center for Astrophysics, 60 Garden St., Cambridge, MA 02138 USA; javier@head.cfa.harvard.edu, jem@cfa.harvard.edu, jsteiner@head.cfa.harvard.edu

<sup>2</sup> MIT Kavli Institute for Astrophysics and Space Research, MIT, 70 Vassar Street, Cambridge, MA 02139, USA; grinberg@space.mit.edu

<sup>3</sup> Department of Physics & Center for Space Science and Technology, UMBC, Baltimore, MD 21250, USA

<sup>4</sup> CRESST & NASA Goddard Space Flight Center, Greenbelt, MD 20771, USA; katja@milkyway.gsfc.nasa.gov

<sup>5</sup> Center for Astrophysics and Space Sciences, University of California at San Diego, La Jolla, CA, USA, rrothschild@ucsd.edu

<sup>6</sup> <http://heasarc.gsfc.nasa.gov/docs/xte/whatsnew/big.html>

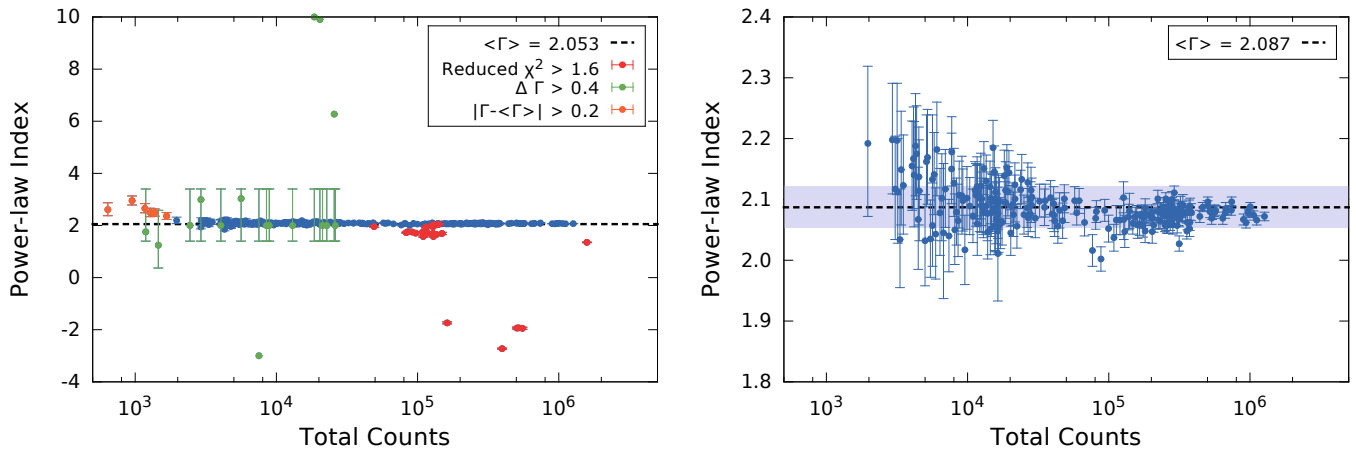


FIG. 1.— Photon power-law index vs. the number of counts in a Cluster B spectrum of the Crab. Results for the complete sample of 283 spectra are shown in the left panel and results for the selected sample of 230 spectra in the right panel. The dashed lines and shaded regions indicate the average value and  $\pm 1$  standard deviation, respectively.

2006 the mechanism that rocked Cluster A failed and the cluster was parked in the on-source position. (3) In March 2010 the mechanism that rocked Cluster B also failed (having completed several millions cycles and far exceeded its design goal). We consider only data that were taken when the instruments were actively rocking because the analysis of HEXTE data that lack quasi-simultaneous measurements of the background is problematic (Pottschmidt et al. 2006).

Our analysis and discussion are focused on Cluster B because, unlike Cluster A, it shows pronounced residual features; furthermore, it was active  $\approx 4.3$  years longer than Cluster A. For Cluster A we provide only a summary of results (Section 5).

During the mission, 283 individual pointed observations of the Crab were performed with HEXTE Cluster B. All the spectra for both clusters have been extracted using the standard tools in HEASOFT 6.16 and corrected for deadtime using the `hxtdead` tool. Visual inspection of the data, preliminary power-law fits to the spectra, and information available at the HEASARC revealed that for some observations the source was occulted by the Earth or that the data were acquired in a non-standard mode (e.g., the data corresponding to proposal P50100 lacks coverage below  $\sim 30$  keV). Such data were excluded.

We analyzed each of the 283 observations separately. For all of our model fitting and statistical analysis, we used XSPEC 12.9.0d (Arnaud 1996). Working with the data as grouped by the standard reduction procedure, we further binned the data to  $\sim 3$  channels per resolution element. Specifically, using ISIS 1.6.2 (Houck 2002) we binned up the data<sup>7</sup> by factors of 2, 3, and 4, in the energy ranges 20–30 keV, 30–40 keV, and 40–250 keV, respectively. No allowance was made for systematic error in the response of the detector. Each spectrum was fitted using a power-law model, with its photon index  $\Gamma$  and normalization as the only two fit parameters.

Because a break in the Crab spectrum has been reported by several observers, we also alternatively fitted

our data using a broken power-law model. However, for nearly all of the spectra the break energy was unconstrained. Furthermore, the combined ratio spectrum (discussed below) differed only very slightly from that derived using the single-slope model. For simplicity, we therefore adopted the unbroken power-law model. For details, see Section 6.

The left panel in Figure 1 shows for each of the 283 spectra the recovered power-law photon index  $\Gamma$  vs. the total number of counts. We discard three categories of data for which: the fit is relatively poor with  $\chi^2_{\nu} > 1.6$  (red points); the uncertainty in  $\Gamma$  exceeds 0.4 (green points); and  $\Gamma$  is more than 0.2 above or below its mean value of  $\langle \Gamma \rangle = 2.053$  (orange points). The poor fits in the first category evidently result from background exposure times that are anomalously short, typically only 3% of the respective source exposure time.

With the exclusion of these data, our final sample for Cluster B is comprised of 230 spectra which contains a total of 39 million counts. The right panel in Figure 1 shows for these selected spectra the power-law index vs. the total number of counts. The modest variability in the photon index is comparable to that found for the PCA by us (García et al. 2014) and by Shaposhnikov et al. (2012). We note that long-term variations in the flux and photon index of the Crab have been reported by Wilson-Hodge et al. (2011). Attempting to corroborate these results is beyond the scope of this paper. Meanwhile, these variations do not affect our results (i.e., the performance of our correction tool) because we fit each observation independently.

We now combine all 230 Cluster-B Crab spectra to produce the three “total counts spectra” shown in Figure 2. The counts in channel  $i$  for the source spectrum is the sum over the individual spectra  $j$  of the background-subtracted source counts  $S_i = \sum_j S_{i,j}$ . The background and model spectra are similar sums over the background counts ( $B_i = \sum_j B_{i,j}$ ) and model counts ( $M_i = \sum_j M_{i,j}$ ). We emphasize that the model here is not a fit to the summed spectrum, but rather it is the sum of the models fitted to the 230 individual spectra. At energies  $\gtrsim 140$  keV the background is dominant. In the highest channel at 250 keV, there are  $\sim 100,000$

<sup>7</sup> Whether one bins the data using ISIS or GRPPHA is unimportant; both tasks define the groupings in the PHA source file, while the background and response files remain unchanged.

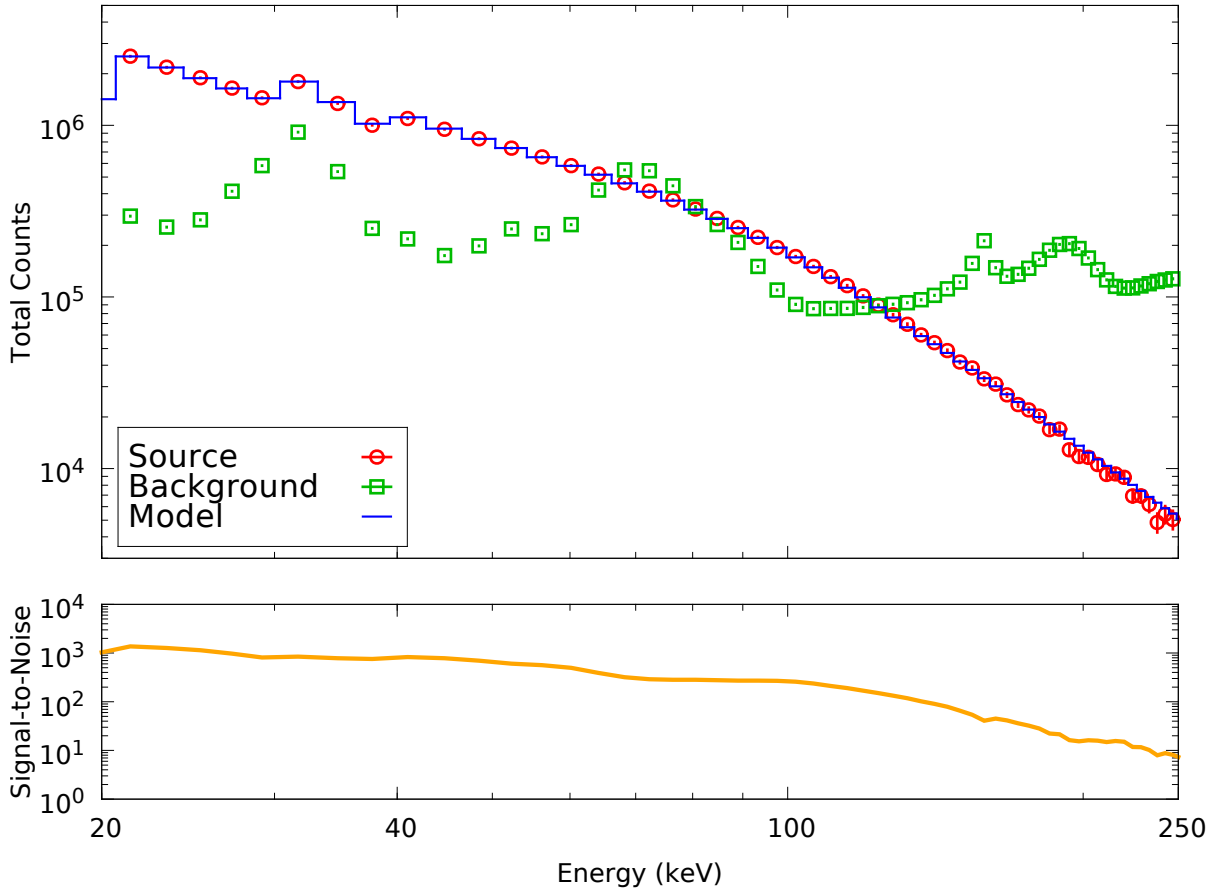


FIG. 2.— (top) Total counts spectra for the source, background and model produced using all 230 Crab observations for HEXTE Cluster B. (bottom) Significance of the signal, which for each channel individually is the total source counts divided by its uncertainty.

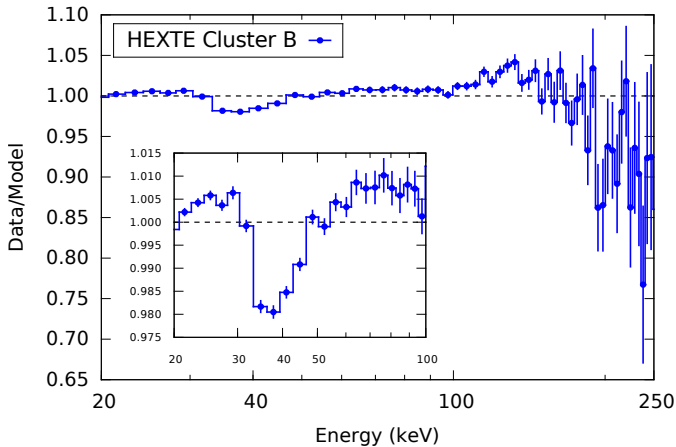


FIG. 3.— Ratio spectrum for Cluster B created by combining the residual spectra produced by fitting individually our complete sample of 230 selected Crab spectra.

background counts and only  $\sim 5,000$  source counts.

The error bars for the source and background spectra in Figure 2 are plotted, but they are minuscule and scarcely visible. For the source spectrum, the statistical uncertainty in the number of counts in channel  $i$  is

$$\sigma_i = \sqrt{S_i + (T_o/T_b)B_i + (T_o/T_b)^2 B_i}, \quad (1)$$

where  $T_o$  and  $T_b$  are respectively the exposure times for the observation of the source (and its background) and for the observation of the background alone. The significance of the detection in each channel (i.e., the signal-to-noise ratio), which is shown in the lower panel of Figure 2, is simply

$$(SNR)_i = S_i/\sigma_i. \quad (2)$$

The ratio spectrum  $S_i/M_i \pm \sigma_i/M_i$  is shown in Figure 3. Its most distinctive feature is a  $\approx 1\%$  dip that extends from about 30 keV to 50 keV, which coincides with the iodine K-edge at 33.17 keV (Wayne et al. 1998). Additional features that are less significant are present above 100 keV. At this point we could adopt the ratio spectrum in Figure 3 as a final product to be used in correcting HEXTE spectra for Cluster B. However, via the iterative process described in the following section we obtain a final product of much higher quality, which we refer to hereafter as the “correction curve.”

### 3. CORRECTION CURVE FOR CLUSTER B AND THE CALIBRATION TOOL HEXBCORR

We now produce the correction curve for Cluster B following precisely the procedures we used earlier for the PCA, which are extensively described in Section 4 in García et al. (2014). Producing a correction curve for the HEXTE is simpler than for the PCA because the HEXTE automatic gain control held the gain fixed

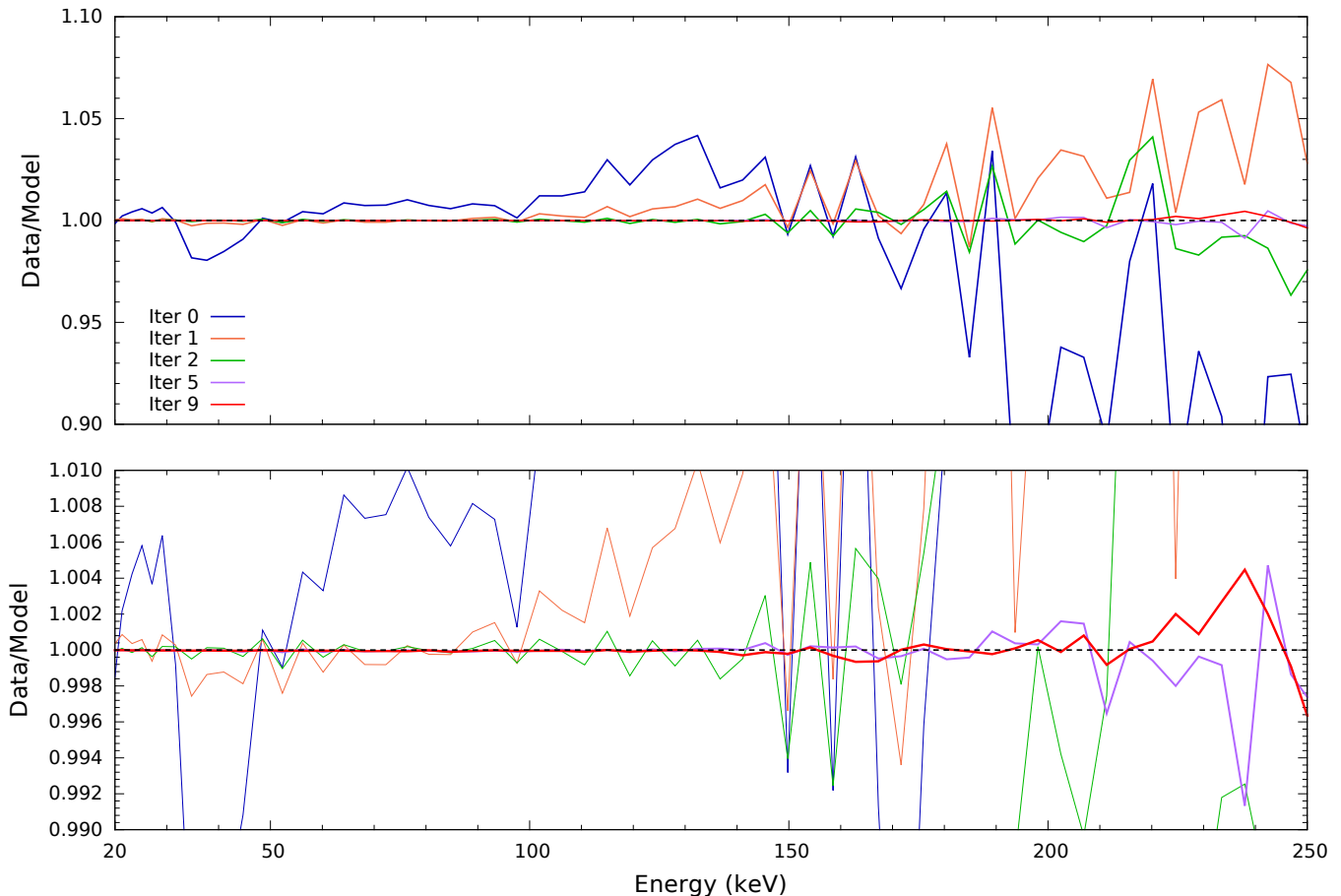


FIG. 4.— A succession of Cluster B ratio spectra (which were created by the iterative process described in the text) displayed over the full 20–250 keV band. (*top*) The parent ratio spectrum, the blue curve labeled `iter=0`, is identical to the ratio spectrum plotted in Figure 3. Four of the nine smaller-amplitude daughter spectra are shown, including that generated by the tenth and final iteration (the red curve labeled `iter=9`). (*bottom*) The same ratio spectra more sensitively displayed.

throughout the mission so that every observation has the same energy-to-channel mapping.

In brief: We start with the ratio spectrum shown in Figure 3, which is identical to the curve labeled `iter=0` in Figure 4 except that the error bars have been suppressed. We then correct our 230 spectra by dividing each one by this ratio spectrum and repeat the process described in the previous section, thereby creating a new ratio spectrum that is labeled `iter=1` in Figure 4. The procedure is repeated a total of 10 times, resulting in the red curve labeled `iter=9`, after which additional iterations do not produce significant changes in the curve. The panels in Figure 4 show at two different scales the reduction in the amplitude of the residual features achieved at several points in the iteration process over the full energy range (20–250 keV). The top panel highlights the gross improvements achieved in the first few iterations, and the lower panel shows in detail how each successive iteration reduces further the amplitude of every residual feature in the spectrum.

We repeated the analysis described above, this time including a correction for the normalization using the model `recorn` in XSPEC. We find that the addition of this model component has a very small effect on the ratio spectrum in Figure 3, producing only mild effects ( $\lesssim 2\sigma$ ) at energies above 100 keV. The effect is negligible

in practice for the correction of HEXTE data, and for simplicity we do not use `recorn` in our analysis.

The final correction curve for Cluster B is the product of all 10 correction curves (five of which are plotted in Figure 4). This final correction curve, plotted in Figure 5, constitutes the calibration tool `HEXBCORR`. To correct any Cluster B object spectrum of interest one simply divides the counts in each energy channel, as well as the error, by the corresponding value of the correction curve.

#### 4. TESTING THE TOOL `HEXBCORR` ON SPECTRA OF STELLAR-MASS BLACK HOLES

As a test of the calibration tool `HEXBCORR`, we apply it to composite spectra of two bright transient Galactic black holes: XTE J1752–223 and GX 339–4. For both sources, the Cluster B data were collected in the bright hard state, and the spectra each contain several million counts. Our analysis is aimed at demonstrating the efficacy of `HEXBCORR`, and we do not concern ourselves with employing an accurate physical model.

**XTE J1752–233:** We selected 57 Cluster B observations (all the data for proposal numbers 94044 and 94331). We combined the spectra in two steps. First, we created a summed residual spectrum precisely as we did for the Crab, as described in Section 2. Secondly,

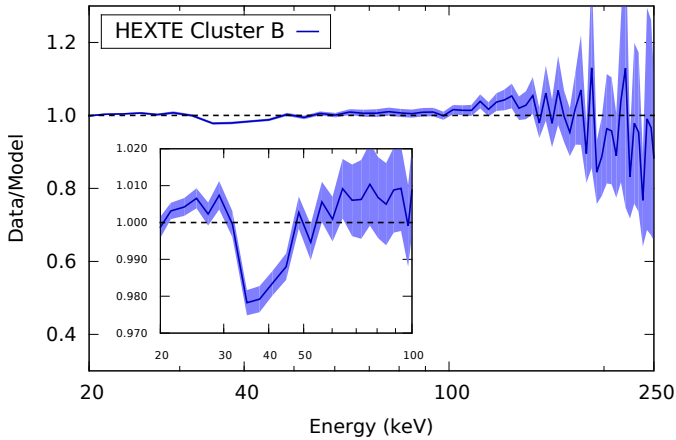


FIG. 5.— Final correction curve for Cluster B. The lighter shaded region bounding the curve shows the  $1\sigma$  level of statistical error.

we then added back in to this spectrum the average continuum component, which we generated synthetically using the average values of the spectral index and normalization parameter, and using the appropriate exposure time for the summed spectrum. A detailed description of this process, and the rationale for combining spectra in this way, is given in Section 3 of [García et al. \(2015\)](#). The summed spectrum contains a total of 10.4 million counts in the energy range 20–250 keV. We applied the tool `HEXBCORR` to the spectrum by simply dividing the source counts, and errors, by the correction curve shown in Figure 5. We then fitted both the original (uncorrected) and the corrected spectra using a cutoff power-law model. The residuals are compared in the left panel of Figure 6, which shows the contributions to  $\chi^2$  for each channel. The effect of the correction is clear-cut. In particular, the strong 30–50 keV feature, present in the original spectrum and in the Crab spectrum (Figure 3), is completely absent in the corrected spectrum. Furthermore, the tool reduces the residuals at almost every energy. The reduction in total  $\chi^2$  is striking:  $\chi^2 = 205.1$  to  $\chi^2 = 68.3$  ( $\Delta\chi^2 = 136.8$  with 54 degrees of freedom in both cases). At the same time, the model parameters change only slightly: the photon index from  $1.23 \pm 0.01$  to  $1.18 \pm 0.01$ ; the cutoff energy from  $125.7 \pm 2.4$  keV to  $111.9 \pm 1.9$  keV; and the normalization from  $0.26 \pm 0.01$  to  $0.23 \pm 0.01$  (where the first quantity is the value for the original spectrum).

**GX 339–4:** We used the exceptionally bright hard-state Cluster B data collected in 21 observations made during 2002 April 20–30, which correspond to the data defined by Box A in [García et al. \(2015, see their Figure 1\)](#). The combined spectrum contains a total of 5.6 million counts. We again fitted both the original and corrected data using the same power-law model with a high energy cutoff; an additional mild cutoff was required at low energies in order to achieve a good fit. As before, we do not seek a physical description of these data; rather we apply a simple phenomenological model of the continuum. The residuals are compared in the right panel of Figure 6, which shows the contributions to  $\chi^2$  for each channel. Once again, strong residual features near 40 keV that are present in the uncorrected spectrum are largely eliminated by the application of `HEXBCORR`.

The improvement in the fit is quite significant, although less so than in the previous example:  $\chi^2 = 392.1$  for the uncorrected spectrum and  $\chi^2 = 337.0$  for the corrected spectrum (i.e.,  $\Delta\chi^2 = 55.1$  with 53 degree of freedom in both cases), while the model parameters in this case are consistent within the uncertainties. For the original and corrected spectra, respectively, the photon index is  $1.65 \pm 0.03$  and  $1.60 \pm 0.03$ ; the high energy cutoff is  $73.0 \pm 2.5$  and  $67.0 \pm 2.2$ ; and the normalization is  $2.3 \pm 0.2$  and  $2.1 \pm 0.2$ . In comparison with the results for XTE J1752–223, the consistency of the fit parameters and smaller value of  $\Delta\chi^2$  for GX 339–4 can be reasonably explained by noting that its spectrum contains only about half as many counts.

## 5. FITS TO CRAB SPECTRA AND THE CREATION OF A RATIO SPECTRUM FOR CLUSTER A

We performed precisely the same global analysis of the Crab data for Cluster A that we performed for Cluster B. As in Section 2, we fitted all the available data for Cluster A, in this case 204 observations; fitted the spectra with a simple power-law model; applied the same selection criteria; and arrived at our final data sample of 168 spectra comprising a total of 37 million counts. Again, following the procedures described in Section 2, we produced a data-to-model ratio spectrum that is a sum of all the selected data. This ratio spectrum for Cluster A is compared to that of Cluster B in Figure 7. There are no significant residual features in the spectrum of Cluster A, which is an unexpected result given that the clusters were built to the same design. The residuals at all energies are approximately consistent with counting statistics. We conclude that it is unnecessary to correct Cluster A data.

We tested the quality of raw (i.e., uncorrected) Cluster A data for GX 339–4 by making a direct comparison with the corrected Cluster B spectrum of this source shown in Figure 6. (Note that no rocked Cluster A data are available for XTE 1752–233; see Section 2.) We generated the Cluster A spectrum of GX 339–4 using precisely the same procedures used for the Cluster B spectrum (Section 4), and we fitted both spectra independently using the same cutoff power-law model. The fit residuals for the two spectra are compared in Figure 8. The quality of the fits is very similar, and all the model parameters are consistent within the uncertainties. The total  $\chi^2$  is slightly worse for the Cluster A spectrum ( $\chi^2 = 332.7$  vs.  $\chi^2 = 371.43$ ), but this is likely largely because the number of counts is greater (7.7 million vs. 5.6 million). Thus, we find that the uncorrected Cluster A data are comparable in quality to the corrected Cluster A data, confirming our conclusion above that it is unnecessary to correct Cluster A data.

## 6. DISCUSSION AND CONCLUSIONS

Cluster A data are free of the instrumental features that require correction in the Cluster B data. This is surprising if these features are instrumental because one would expect the performance of these essentially identical clusters to be more nearly similar. While the reason for the dissimilarity is unclear, the leading hypothesis is that it resulted from adjusting Cluster B’s calibration two months into the mission, which was necessitated by

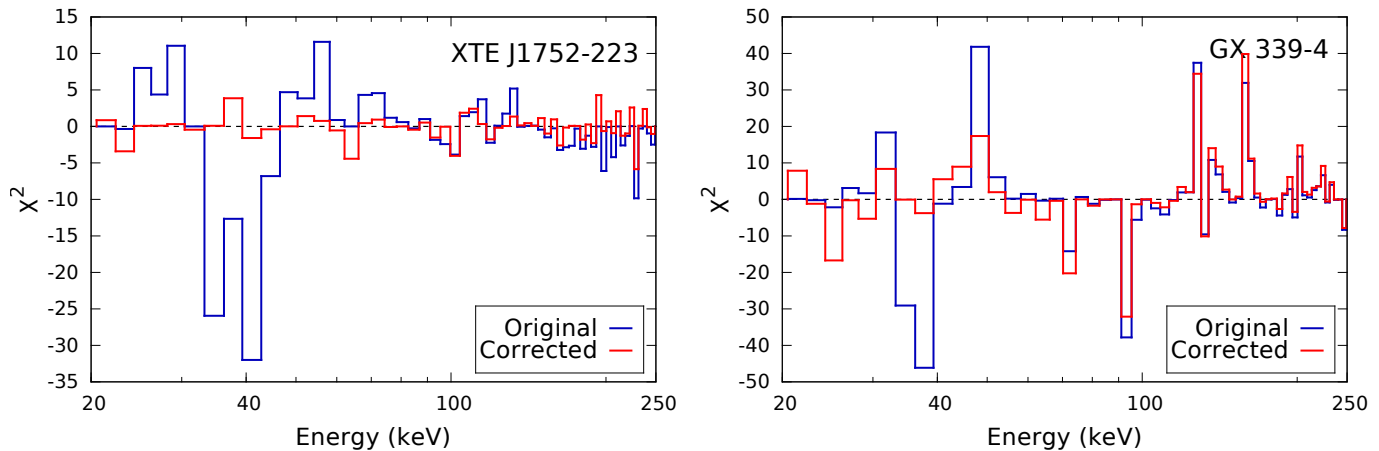


FIG. 6.— Comparison of the residuals from the fits to the original and the corrected data for XTE J1752–223 (left panel) and GX 339–4 (right panel).

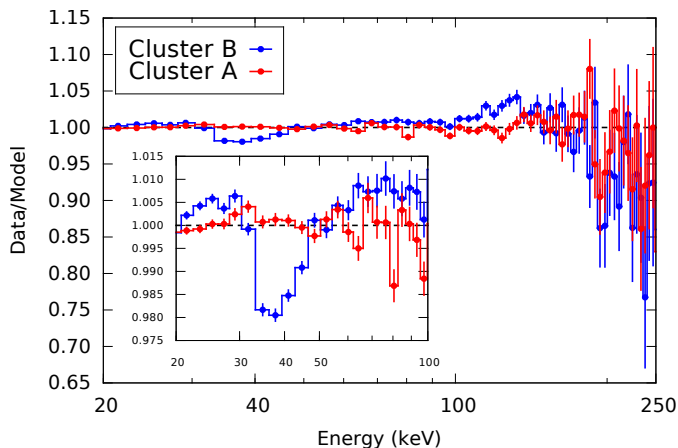


FIG. 7.— Comparison of the residuals for the two clusters from fits to the Crab data. The blue spectrum for Cluster B is identical to that shown in Figure 3.

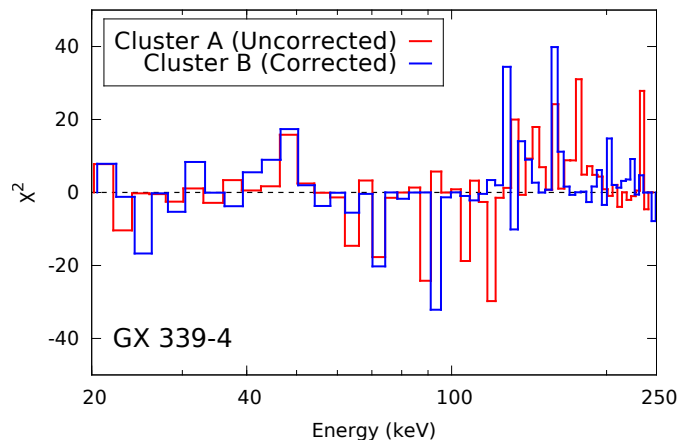


FIG. 8.— Comparison of the residuals for the two clusters from fits to the combined spectrum of GX 339–4 with 5.6 million counts.

the failure of one of its four detectors (see Section 2). Unfortunately, the Crab data collected prior to the failure are too sparse to corroborate this hypothesis. Since the Brookhaven calibration was done with a single HEXTE detector, it is possible that one or more cluster B detectors had a slightly different response at and just beyond the K-edge of iodine, and that is the source of the residual, since the same two segment description of the edge response was used for all detectors.

The calibration of the HEXTE depends on both laboratory and in-flight data. The efficiency of the detectors vs. energy was determined prior to launch using radioactive sources and monochromatic X-rays generated at Brookhaven National Laboratory. This part of the instrument response includes the energy-dependent escape of photons above the K edge of iodine. The efficiency vs. energy above and below the edge was mimicked by two line segments, which is an imperfect model because the profile of the edge is more complicated than a step function.

The final calibration of the open area and point spread function (PSF) of the instruments was determined post-launch using Crab data. Multiple observations were made on-axis and over a range of off-axis angles. These

data were used to adjust the preliminary laboratory measurements of the PSF and open area. None of these individual Crab observations was sensitive enough to detect the 1% dip seen in the combined ratio plot (Figure 3). The adjustments to the calibration of Cluster B after the detector failure were solely to the open area and the PSF; the detector efficiencies were left unchanged. These adjustments are the most significant event that differentiates the two HEXTE clusters. However, it remains an open question precisely how this event could produce the relatively large residuals in Cluster B that are absent in Cluster A.

As noted in Section 2, in creating the tool HEXBCORR we analyzed all the Crab data using a simple absorbed power-law model while ignoring the evidence that the spectrum breaks at an energy that is quite uncertain:  $79 \pm 10$  keV (Strickman et al. 1979),  $128 \pm 4$  keV (Jung 1989),  $60 \pm 7$  keV (Bartlett 1994)  $57 \pm 3$  keV (Rothschild et al. 1998), 100 keV (fixed) (Jourdain & Roques 2009),  $105 \pm 20$  keV and  $117 \pm 19$  keV (Yamada et al. 2011). In addition to these reports of a break, we note that our ratio spectrum in Figure 3 and our final correction curve in Figure 5 show marginal evidence for a break at energies  $\gtrsim 150$  keV, although this apparent defect in our correction curve is relatively unimportant because

spectra contain few source counts at these energies and the background is the dominant source of uncertainty.

As an alternative to the simple power-law model, we fitted our 283 Cluster-B spectra using a broken power-law model, but we obtained unsatisfactory results; namely, for nearly all the spectra the break energy was unconstrained with values scattered randomly across the allowed range of 50–200 keV. Most importantly, the net ratio plot for these fits was only marginally different from that obtained using the simple power-law model, which accurately captures the important  $\sim 1\%$  dip at  $\sim 40$  keV and the other principal features in the ratio spectrum (Figure 3). Therefore, all of our results are based on the simple power-law model.

Our results for XTE J1752–223 and GX 339–4 indicate that for combined spectra of bright sources, which are comprised of dozens of individual spectra and contain several million counts, the application of HEXBCORR significantly improves the quality of the fit to Cluster B data, while having at most a modest effect on broadband spectral parameters. For example, for the latter source with 5.6 million counts the values of the photon index, cutoff energy, and normalization were consistent within the statistical uncertainties. For XTE J1752–223 with 10.4 million counts, the parameters changed modestly, but by several standard deviations: the photon index, cutoff energy and normalization changed by  $\Delta\Gamma = 0.05 \pm 0.01$ ,  $\Delta E = 13.8 \pm 3.1$  keV, and  $\Delta N = 0.03 \pm 0.01$ . For an individual spectrum of a bright source with an exposure time of only a few ks, it is likely that the correction is at most cosmetic with essentially no effect on the broadband parameters.

However, the correction is potentially important for the study of spectral features such as cyclotron lines, particularly those at energies of  $\sim 30 - 50$  keV. There have been a number of reports of cyclotron lines in this band, some based on HEXTE data (e.g., Heindl et al. 1999b; Coburn et al. 2001; Heindl et al. 2001, 2003; Rodes-Roca et al. 2009; Tsygankov et al. 2012). The instrumental features we detect have an amplitude of about 1%, which is much less than that of a typical cyclotron line. However, in some cases the application of our calibration tool may prove fruitful. For example, DeCesar et al. (2013), who discovered a 10 keV cyclotron line (with an amplitude  $\sim 3\% - 10\%$ ) in the spectrum of Swift J1626.6–5156, find residual features in their PCA and HEXTE (Cluster B) spectra at  $\sim 40$  keV. The authors argue that these features are instrumental and not a harmonic of the 10 keV line, an hypothesis that can possibly be tested using our calibration tool. A spectrum of the bursting pulsar GRO J1744–28 provides a second example where a residual feature was interpreted as an instrumental artifact rather than as a cyclotron line (Heindl et al. 1999a). The question of whether our calibration tool is actually important for the study of cyclotron lines is beyond the scope of this paper.

The benefits of correcting HEXTE Cluster-B data with HEXBCORR are greatest for spectra with many counts. Figure 9 roughly quantifies this benefit by plotting the improvement in the fit achieved by application of the tool to the brighter Crab spectra as a function of the total counts. The effect of the correction becomes apparent for spectra with  $\sim 10^5$  counts and it becomes quite significant as the number of counts approaches  $10^6$ . The

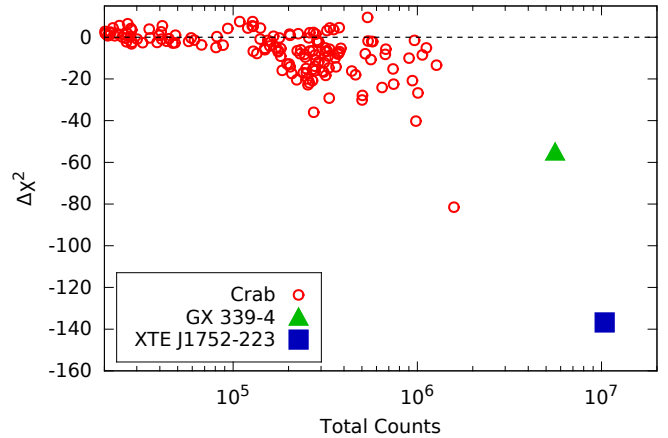


FIG. 9.— Improvement in the fit for Cluster-B data, as measured by a decrease in  $\chi^2$ , as a function of total counts for bright spectra of the Crab and for summed spectra of GX 339–4 and XTE J1752–224. The Crab spectra were fitted over the 20–250 keV band using the simple absorbed power-law model. The results shown for the two black hole sources are those given in Section 4.

improvement in the fit for the spectra of GX 339–4 and XTE J1752–228 with several million counts apiece is dramatic. The figure indicates the value of making the correction for spectra with more than  $\sim 10^5$  counts. This limit should be considered only a useful rule of thumb since it likely depends on the spectral shape.

In summary, we have demonstrated that a mission-averaged spectrum of the Crab with 39 million counts in the HEXTE band reveals imperfections in the calibration of Cluster B. Following a procedure designed originally for correcting PCA data, we show how to reduce the principal  $\sim 30-50$  keV instrumental feature in Cluster B data by an order of magnitude, while significantly reducing the residuals at nearly all energies in the full 20–250 keV band. To correct any Cluster B spectrum of interest one applies the tool HEXBCORR, which divides the spectrum, channel-by-channel, with the correction spectrum shown in Figure 5. We show that for combined spectra of bright sources containing more than  $10^5$  counts, the correction greatly improves the quality of the fit while only mildly affecting the broadband fit parameters. For individual spectra of bright sources with many fewer counts, the effects on the broadband parameters will be correspondingly less. However, for the study of discrete spectral features at energies of  $\sim 30-50$  keV, such as cyclotron lines, the correction may be important even for individual spectra. Finally, we find no significant residual features in the combined Crab spectrum using Cluster A observations, and we conclude that no correction is required for these data. Earlier, we made publicly available the calibration tool PCACORR for correcting PCA data (García et al. 2014). Now, the correction curve for HEXTE Cluster B along with a Python script, which constitutes the tool HEXBCORR, is publicly available at <http://hea-www.cfa.harvard.edu/~javier/hexBcorr/>.

We thank an anonymous referee for several helpful comments. JG and JEM acknowledge the support of a CGPS grant from the Smithsonian Institution. JFS has been supported by NASA Hubble Fellowship grant HST-HF-51315.01 and NASA Einstein Fellowship grant

PF5-160144. VG acknowledges support provided by NASA through the Smithsonian Astrophysical Observatory (SAO) contract SV3-73016 to MIT for support of the

Chandra X-Ray Center (CXC) and Science Instruments; CXC is operated by SAO for and on behalf of NASA under contract NAS8-03060.

## REFERENCES

- Arnaud, K. A. 1996, in *Astronomical Society of the Pacific Conference Series*, Vol. 101, *Astronomical Data Analysis Software and Systems V*, ed. G. H. Jacoby & J. Barnes, 17 [2](#)
- Bartlett, L. M. 1994, PhD thesis, UNIVERSITY OF MARYLAND COLLEGE PARK. [6](#)
- Coburn, W., Heindl, W. A., Gruber, D. E., et al. 2001, *ApJ*, 552, 738 [6](#)
- DeCesar, M. E., Boyd, P. T., Pottschmidt, K., et al. 2013, *ApJ*, 762, 61 [6](#)
- García, J. A., McClintock, J. E., Steiner, J. F., Remillard, R. A., & Grinberg, V. 2014, *ApJ*, 794, 73 [1](#), [2](#), [3](#), [6](#)
- García, J. A., Steiner, J. F., McClintock, J. E., et al. 2015, *ApJ*, 813, 84 [4](#)
- Heindl, W., Blanco, P., Gruber, D., et al. 1999a, *Nuclear Physics B Proceedings Supplements*, 69, 216 [6](#)
- Heindl, W., Coburn, W., Kreykenbohm, I., & Wilms, J. 2003, *The Astronomer's Telegram*, 200, 1 [6](#)
- Heindl, W. A., Coburn, W., Gruber, D. E., et al. 1999b, *ApJ*, 521, L49 [6](#)
- . 2001, *ApJ*, 563, L35 [6](#)
- Houck, J. C. 2002, in *High Resolution X-ray Spectroscopy with XMM-Newton and Chandra*, ed. G. Branduardi-Raymont [2](#)
- Jahoda, K., Markwardt, C. B., Radeva, Y., et al. 2006, *ApJS*, 163, 401 [1](#)
- Jourdain, E., & Roques, J. P. 2009, *ApJ*, 704, 17 [6](#)
- Jung, G. V. 1989, *ApJ*, 338, 972 [6](#)
- Levine, A. M., Bradt, H., Cui, W., et al. 1996, *ApJ*, 469, L33 [1](#)
- Pottschmidt, K., Rothschild, R. E., Gasaway, T., Suchy, S., & Coburn, W. 2006, in *Bulletin of the American Astronomical Society*, Vol. 38, *AAS/High Energy Astrophysics Division #9*, 384 [2](#)
- Rodes-Roca, J. J., Torrejón, J. M., Kreykenbohm, I., et al. 2009, *A&A*, 508, 395 [6](#)
- Rothschild, R. E., Blanco, P. R., Gruber, D. E., et al. 1998, *ApJ*, 496, 538 [1](#), [6](#)
- Shaposhnikov, N., Jahoda, K., Markwardt, C., Swank, J., & Strohmayer, T. 2012, *ApJ*, 757, 159 [2](#)
- Strickman, M. S., Johnson, W. N., & Kurfess, J. D. 1979, *ApJ*, 230, L15 [6](#)
- Tsygankov, S. S., Krivonos, R. A., & Lutovinov, A. A. 2012, *MNRAS*, 421, 2407 [6](#)
- Wayne, L. R., Heindl, W. A., Hink, P. L., & Rothschild, R. E. 1998, *Nuclear Instruments and Methods in Physics Research A*, 411, 351 [2](#)
- Wilson-Hodge, C. A., Cherry, M. L., Case, G. L., et al. 2011, *ApJ*, 727, L40 [2](#)
- Yamada, S., Makishima, K., Nakazawa, K., et al. 2011, *PASJ*, 63, 645 [6](#)